THE ASTROPHYSICAL JOURNAL, 360:95–105, 1990 September 1

SUBARCSECOND RESOLUTION OBSERVATIONS OF THE CENTRAL PARSEC OF THE GALAXY AT 2.2 MICRONS

M. SIMON,[1,2] W. P. CHEN,[1,2] W. J. FORREST,[2,3,4] J. D. GARNETT,[2,3,4]
A. J. LONGMORE,[5] T. GAUER,[5] AND R. I. DIXON[6]

Received 1989 October 5; accepted 1990 March 1

ABSTRACT

We have observed four lunar occultations of the Galactic center in the infrared K band, three with infrared cameras and one by high-speed photometry. The occultation observations enable us to estimate the sizes of objects brighter than $K \sim 10$ mag in the central parsec of the Galaxy, and, for objects brighter than $K \sim 11$, to separate them from their surroundings and to measure their fluxes. Of the relatively bright K-band sources within 3″ of Sgr A*, IRS 16NE, 16NW, and 29 are smaller than ~510 AU, and IRS 16C and a compact component of IRS 16SW are smaller than 85 AU. They are probably stars. About half the flux from this central 3″ radius region is diffuse emission that is probably contributed by an unresolved cluster of stars. There is no peak of K-band emission at Sgr A* to a limit of about 10.6 mag. IRS 1W and 13 are resolved into pairs of sources; they are probably the stars that excite these H II regions. IRS 7 is smaller than 100 AU. It has a faint companion. The shape of the luminosity functions for the central pc^2 and the central ~150 pc^2 (Lebofsky and Rieke) are similar.

Subject headings: galaxies: The Galaxy — galaxies: nuclei — infrared: sources — occultations

I. INTRODUCTION

The center of our Galaxy is heavily obscured, so it cannot be observed in visible light. Radio and infrared observations have revealed that the central parsec contains a high density of stars, ionized gas, a mass of $\sim 10^6\ M_\odot$, and, at or very near the dynamical center, the unresolved nonthermal radio source Sgr A* (Backer and Sramek 1987; Rieke, Rieke, and Paul 1989, hereafter RRP; McGinn *et al.* 1989). The IRS 16 complex of near-infrared sources is of particular interest because its components lie within ~2″ of Sgr A* and thus are probably in its immediate vicinity. The colors of its components seem to be very blue, but their nature is unknown (RRP). Tollestrup, Capps, and Becklin (1989, hereafter TCB) give a description of the near-infrared appearance of the region. Throughout this paper, we assume 8.5 kpc for the distance to the Galactic center (Kerr and Lynden-Bell 1986), so 1″ corresponds to 8500 AU.

The 1986–1989 series of lunar occultations of the Galactic center offered a unique opportunity to study the infrared sources at very high angular resolution. A considerable effort was made, therefore, to observe as many of the occultations as possible. Considerations of source brightness, the requirement to take data rapidly, and instrumental sensitivity indicated the infrared K band, which is centered at 2.2 μm, as the best spectral region in which to observe.

Adams *et al.* (1988) observed the occultation at La Palma, Canary Islands, on 1986 September 11. By high-speed photometry of the IRS 16 complex at K, they found that ~60% of the flux in a 6″.5 aperture came from four discrete sources and the rest from diffuse emission. Three of the discrete sources were found to be smaller than 50 milliarcseconds (mas), while the fourth was resolved and about 300 mas in extent (see also Simons, Becklin, and Hodapp 1989). The extended object was identified with IRS 16NE, but the lunar limb orientation of this event was such that it was not possible to identify the features unambiguously. Since high-speed photometry through an aperture yields a one-dimensional intensity distribution that is the projection, in the occultation direction, of the actual two-dimensional structure, source identification in a complex field can be difficult.

The development of infrared cameras offered a solution to this problem. McLean *et al.* (1987) pioneered occultation observations with an IR camera in the 1987 January 26 Galactic center event at Mauna Kea. Their preliminary results, also at K, showed vividly how a time series of images could identify which sources in a crowded field were occulted at a given moment. Their results also demonstrated the sensitivity of IR cameras and their capability to accommodate to situations of high and variable background.

This paper presents the results of our K-band observations of four Galactic center occultations at Mauna Kea. Three were observed with infrared cameras—one using the facility instrument at the United Kingdom Infrared Telescope (UKIRT), and two using the University of Rochester infrared camera at the Canada-France-Hawaii Telescope (CFHT) and the NASA Infrared Telescope Facility (IRTF). These data provide size information and fluxes not only for the IRS 16 complex but also for the relatively bright sources in the central parsec of the Galaxy. The fourth occultation was observed by high-speed photometry at the IRTF and provided higher angular resolution information for the components of IRS 16. Two of the Mauna Kea events were independently observed by Simons *et al.* (1990). Their results, which pertain principally to the IRS 16 region, are in good agreement with ours.

[1] State University of New York at Stony Brook.
[2] Visiting Astronomer at the Infrared Telescope Facility, which is operated by the University of Hawaii under contract from the National Aeronautics and Space Administration.
[3] University of Rochester.
[4] Visiting Astronomer, Canada-France-Hawaii Telescope, CFHT is operated by the National Research Council of Canada, the Centre National de la Recherche Scientifique of France, and the University of Hawaii.
[5] Royal Observatory, Edinburgh.
[6] Edinburgh University.

II. OBSERVATIONS AND INSTRUMENTATION

a) Occultation Circumstances

In the K band, useful occultation observations can be made only at the dark limb of the Moon. The circumstances for the occultations described in this paper are listed in Table 1. The UT date, approximate time of the dark limb occultation of the center of IRS 16, and whether the event was a disappearance (D) or reappearance (R) are given in columns (1) and (2). All the observations were made at Mauna Kea Observatory; the telescope is indicated in column (3). The integration time for the camera images or high-speed photometry are specified in column (4). The contact point position angle, P.A., measured eastward from north, and the predicted occultation rate, $V_\perp$, are given in columns (5) and (6). The apparent velocity of the Moon on the sky, V_m, is given in column (7); $V_\perp = V_m \cos$ (CA), where CA is the contact angle. The actual occultation rate depends on the slope of the limb at the contact point and can be determined from the fringe rate of the Fresnel pattern. Limb slopes are found to be $\leq 30°$ (Evans and Edwards 1980); one standard deviation of the limb slope distribution is about 10°. Since the integrations of the camera observations were not fast enough to resolve the Fresnel pattern, we list in Table 1, column (8), the range of occultation rates that would be produced by limb slopes between $\pm 30°$. The 1988 September 19 occultation was nearly grazing at the northern limb, so the predicted rate was quite slow, and limb slopes could have had a relatively large effect. Possible values of the rate range from 4 times faster than the predicted rate to a negative value, corresponding to a reappearance. Thus, an object could first disappear behind a lunar mountain, then reappear, and finally disappear again for the rest of the occultation.

b) 1987 April 18 Occultation

Observations of the event were made at the UKIRT with the infrared camera IRCAM (McLean *et al.* 1987) which utilizes a Santa Barbara Research Center 58 × 62 pixel InSb array. The plate scale was 0.″62 per pixel, giving a field of view of 36″ × 38″. Limitations on the data transfer rate from the array processor to the VAX11/750 instrument control computer resulted in an exposure time of 260 ms being adopted. In normal sky conditions at 2.2 μm, exposures of this length are read-out noise limited, so decreases in time (hence spatial) resolution are likely to be partly offset by an increase in signal-to-noise ratio. Nine hundred images were obtained, and individually time marked by a signal from a satellite clock. Three hundred frames centered on the IRS 16 occultation event were fully reduced. Until about 10 minutes before the event, the Moon was obscured by thick cloud. A sudden clearance then occurred which lasted until about midway through the occultation. Then the images became progressively more affected by moonlight scattered off encroaching clouds as the fortuitous hole "evaporated." By using quite simple techniques (§ III*c*), it proved possible to recover much of the information on the affected frames despite their initially having a very poor cosmetic appearance.

c) 1988 July 26 Occultation

The event was observed at the CFHT using the University of Rochester IR camera which is also equipped with a Santa Barbara Research Center 58 × 62 pixel InSb array. Pairs of stars of known angular separation were observed at various positions on the array in order to measure the plate scale and image distortion. The plate scale was determined to be 0.″40 per pixel. The image distortion was found to be symmetric about the optical axis, which was nearly centered on the array, and very small, amounting to a radial distortion of at most ~0.8 pixels at the edge of the array. The plate scale provided an effective field of view of ~23″ × 25″, or, at the distance of the Galactic center, ~1 pc^2. An exposure time of 8/60 s was chosen as a reasonable compromise between the competing demands of adequate signal-to-noise and useful time resolution. For the parameters of this event, the limb advanced ~60 mas in each integration. The camera field of view was approximately centered on IRS 16 (see Fig. 1). A series of 900 consecutive images was obtained during the occultation. Cirrus appeared during the occultation but proved not to be a problem.

d) 1988 September 19 Occultation

The occultation occurred in the late afternoon. The Rochester camera was used at the IRTF. The camera plate scale was 0.″3 per pixel. The integration time was 0.5 s, so, on average, the limb advanced ~25 mas per image. The camera was centered on IRS 16, and 1200 images were obtained. Sky transparency was good, but as expected for day time observation, the seeing was worse and more variable than in the July observation.

e) 1989 February 2 Occultation

The occultation occurred shortly after sunrise with excellent sky conditions. It was observed at the IRTF by high-speed photometry using the facility InSb photometer. The photometer was operated direct coupled, that is, without beam switching. A 6″ diameter aperture was used. Shortly before the reappearance, the telescope was offset from a nearby star to a position ~6″ S and ~2″ E of IRS 7, approximately centered on the IRS 16 complex (see Fig. 5). A 1 minute long series of 2 ms integrations centered on the time of reappearance was taken. Immediately after the reappearance, the telescope position was checked by offsetting to IRS 7.

TABLE 1

LUNAR OCCULTATION CIRCUMSTANCES

Date (1)	Time (2)		Telescope (3)	Δt_e (s) (4)	P.A. (5)	$V_\perp$ (arcsec s^{-1}) (6)	V_m (arcsec s^{-1}) (7)	$V'_\perp$ (arcsec s^{-1}) (8)
1987 Apr 18	13^{h}47^m	R	UKIRT	0.260	323°	0.25	0.35	0.09–0.34
1988 Jul 26	11 17	D	CFHT	0.133	86	0.44	0.44	0.33–0.44
1988 Sep 19	3 16	D	IRTF	0.500	15	0.05	0.32	0.20 to −0.12
1989 Feb 2	17 15	R	IRTF	0.002	257	0.33	0.35	0.22–0.35

III. ANALYSIS OF CAMERA DATA AND RESULTS

The IRCAM data and the Rochester Camera data were processed independently at Edinburgh and at Rochester and Stony Brook, respectively. Since the IRCAM and Rochester camera results have important corroborative value when considered separately, we first present the results separately in §§ III*a*, III*b*, and III*c*, and then in § III*d* we consider the photometric and structural information from the three camera observations together.

a) 1988 July and September Occultation Camera Images

Rochester camera data for the two events were processed in the same way. A "dark" exposure taken when the Moon completely covered the field of view at the end of the occultation was subtracted from each image. The array gain was normalized by dividing each image by the image of a flat field. The signal of defective pixels was replaced by the average of all the good pixels. This has only a cosmetic effect, because the Galactic center region had been positioned in the field of view to avoid the defective pixels. The images were inspected to identify when objects disappeared, to obtain a qualitative estimate of the seeing and telescope motion, and, for the July data, to assess the effects of the cirrus. The cirrus signal was very nearly uniform across the image field of view so it could be removed by differential photometry (§ III*b*).

Figure 1 shows the *K*-band image made from the average of three frames taken in the first few seconds of the 1988 July occultation. The frames were selected for good seeing (~0".7). The image was corrected for the very small distortion described in § II*c*. The right ascension and declination axes were set using the coordinates of IRS 7 measured by Forrest, Pipher, and Stein (1986, hereafter FPS) and the plate scale. The position of the nonthermal radio source Sgr A* is plotted at the average position used by TCB; the uncertainty of this determination is ±0".3. We estimate that ±0".5 is the total uncertainty of the coregistration of the IR image and Sgr A*. We reference all fluxes to IRS 7, the brightest object in Figure 1, and we adopt the TCB measurement of its flux, $K = 6.8$ mag.

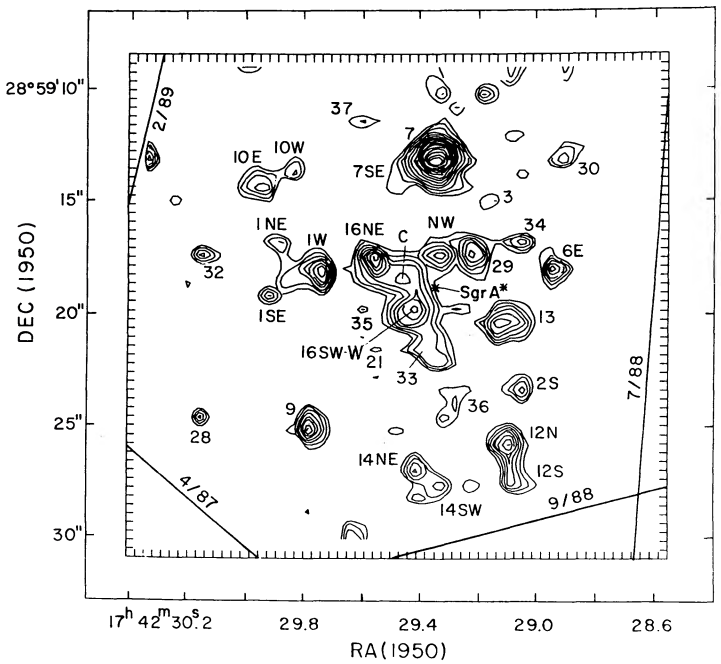

FIG. 1.—The *K*-band image made from the 1988 July occultation data. Identifications of some of the 2 μm sources in the image are marked; the nomenclature follows that of TCB. IRS 7SE and 33 through 37 are new designations. No sources are seen to the west of IRS 6E, because the Moon was already covering that region. The contour intervals are at 0.25 mag intervals. Diagonal straight lines respresent the smooth lunar limb for the four occultations.

We draw attention to the following features of the map:

a) No emission peak coincides with Sgr A*. Because it is so close to the IRS 16 complex, it is difficult to place an upper bound on its flux, but the time series photometry described in § III*b* sets an upper bound of $K \sim 10.6$ mag (3 σ level).

b) The region of IRS 16SW shows a compact peak and low-level extended emission to the east of it. In the notation of TCB, the compact peak is IRS 16SW-W. We label the extended emission 16SWext.

c) A previously undetected source, IRS 7SE, appears ~1".7 E and ~0".9 S with respect to IRS 7 (see also § III*b* and Fig. 2*a*). The *H* and *K* band maps of Simons *et al.* (1990) also show evidence of it.

d) IRS 2S is ~1" S and ~0".4 E of the position given by TCB for IRS 2 which was originally identified at 10 μm by Becklin and Neugebauer (1975, hereafter BN).

e) IRS 13 appears slightly resolved in the east-west direction. The occultation observations resolved it into two objects (§ III*b*).

b) Time Series Photometry from 1988 July and September Occultation Data

The source size and flux were estimated from the 1988 July and September occultation camera data by time series differential photometry. The signal in a 5 × 5 pixel (2" × 2") "aperture" centered on a source was differenced against the average of several nearby positions known to be free of emission. Monitoring the positions of relatively strong sources as the occultation progressed revealed slight image motion caused by seeing and telescope drift. The photometry routine therefore included a centroiding capability to offset the nominal pixel coordinates by the shift of peak emission of a strong source. The photometry for IRS 7 and 9 showed no evidence for time-dependent extinction during the occultations.

The flux of an object is simply proportional to the total change of signal during the disappearance. How rapidly the signal decreases provides an estimate of the size in the occultation direction. Since the camera data do not resolve the Fresnel pattern, the time dependence of the signal can be interpreted geometrically (see Appendix). In each exposure, the limb advances an angular interval $\Delta\theta = V'_\perp \Delta t_e$, where $V'_\perp$ is the actual occultation rate and Δt_e is the exposure time. The fact that $V'_\perp$ cannot be determined from these data is not a serious limitation for interpretation of 1988 July data. Values of $V'_\perp$ that arise from limb slopes less than 30° (which are within three standard deviations of zero slope) are within 25% of the predicted rate (Table 1). Thus, $\Delta\theta$ is in the range 44–60 mas for this event. For sources brighter than $K \sim 10$ mag, it is possible to identify from the time series photometry the *compact* sources which disappear in two images or less, and *extended* sources that take longer to disappear. Sources that are compact in the 1988 July data are smaller than 44–60 mas in the east-west direction (see Appendix). Figure 2*a* shows the time series photometry for some of the brighter sources. IRS 7 is detected at

relatively high signal-to-noise, so it is possible to show that it is smaller than 12 mas (see Appendix).

Interpretation of the time series photometry for the 1988 September event is more difficult than for the July event, because the seeing was more variable and also because of the possibly greater effects of limb irregularities. Both could have made an object flicker off and on as it was occulted, causing it to appear more extended than it really is. The prominent fluctuations of the signal of IRS 7 seen in Figure 2*b* were caused by seeing as identified by direct inspection of the images. The fluctuations that occurred just before the disappearances of IRS 16 Centre and SW (Fig. 2*b*) could have been caused by either seeing or limb irregularities. Nonetheless, objects that appear compact in the sense defined above must be small. Thus, the September data may be used to confirm that the sources identified in the July data as compact are indeed compact.

The results for the 1988 July and September events are summarized in Table 2. Column (1) lists the objects by IRS number. The flux, ratioed to IRS 7, is given in column (2). Assuming $K = 6.8$ mag for IRS 7 (TCB), the corresponding K magnitude is given in column (3). For objects brighter than $K \sim 10$ mag, the compact or extended appearance is described in column (4).

c) 1987 April Occultation Camera Analysis and Results

The UKIRT IRCAM images were reduced slightly differently from those of the Rochester camera. Dark subtraction and flat fielding were done in the same manner. Bad pixels were replaced by the average of all the adjoining pixels.

TABLE 2

1988 JULY AND SEPTEMBER OCCULTATION CAMERA RESULTS

Object (1)	Flux/IRS 7 (2)	m_K (3)	Comments and Size (4)
IRS 1W-W	0.07 ± 0.01	9.7	Western compact
IRS 1W-E	0.11 ± 0.01	9.2	Eastern, compact
IRS 1SE	0.04 ± 0.01	10.3	
IRS 1NE	0.06 ± 0.01	9.9	
IRS 2S	0.04 ± 0.01	10.3	
IRS 3	0.02 ± 0.01	11.1	
IRS 6E	0.07 ± 0.01	9.7	Compact
IRS 7	1.0	6.8	≤12 mas
IRS 7SE	0.03 ± 0.01	10.6	
IRS 9	0.14 ± 0.01	8.9	Compact
IRS 10E	0.07 ± 0.01	9.7	
IRS 10W	0.05 ± 0.01	10.1	
IRS 12N	0.14 ± 0.01	8.9	Compact
IRS 12S	0.07 ± 0.01	9.7	
IRS 13E	0.09 ± 0.01	9.4	Compact
IRS 13W	0.04 ± 0.01	10.3	
IRS 14NE	0.08 ± 0.01	9.5	Compact
IRS 14SW	0.03 ± 0.01	10.6	
IRS 16NE	0.14 ± 0.01	8.9	Compact
IRS 16C	0.05 ± 0.01	10.1	Compact
IRS 16SW-W	0.08 ± 0.01	9.5	Compact
IRS 16SWext	0.08 ± 0.01	9.5	~1″
IRS 16SW (total)	0.16 ± 0.01	8.8	
IRS 16NW	0.05 ± 0.01	10.1	Compact
IRS 21	0.04 ± 0.01	10.3	
IRS 28	0.07 ± 0.01	9.7	Compact
IRS 29	0.07 ± 0.01	9.7	Compact
IRS 30	0.04 ± 0.01	10.3	
IRS 32	0.04 ± 0.01	10.3	
IRS 33	0.04 ± 0.01	10.3	
IRS 34	0.04 ± 0.01	10.3	
IRS 36	0.03 ± 0.01	10.6	

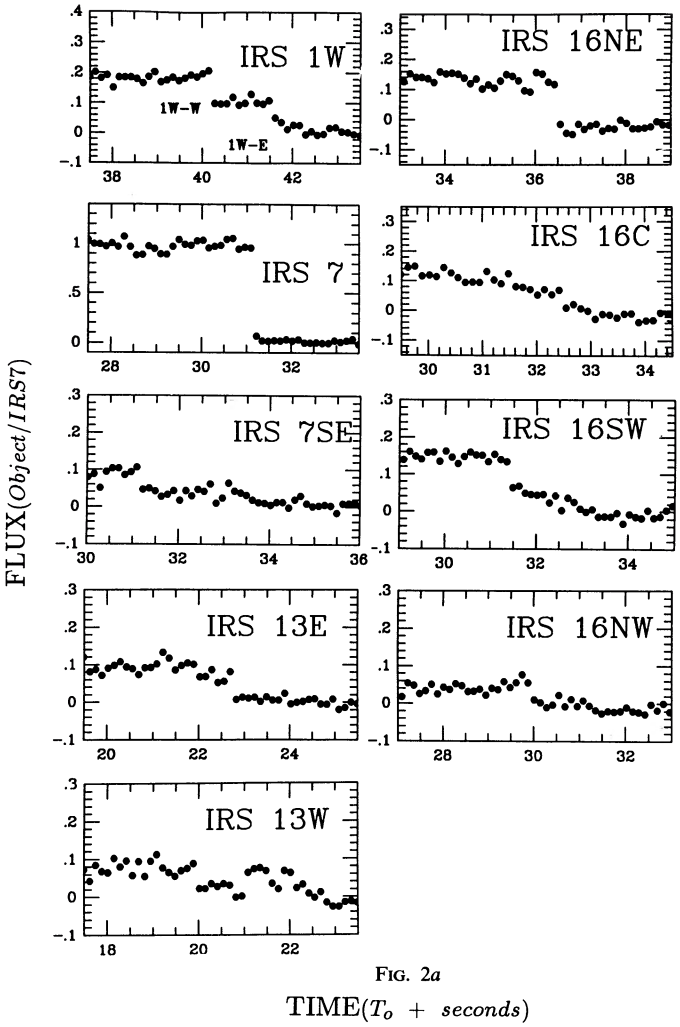

FIG. 2*a*

FIG. 2.—(*a*) Differential photometry for the 1988 July 26 data. In each panel, the ordinate is the flux in the 2″ software aperture ratioed to IRS 7. The time along the abscissae are seconds following a fiducial time T_0. In (*a*), T_0 is 11^h17^m UT. The dots represent 8/60 s integrations. The limb took about 5 s to cross the software aperture in this event. The photometry for each object is approximately centered on its disappearance. (*b*) Differential photometry for the 1988 September 19 data. Same as (*a*), except that T_0 is 3^h10^m UT, the dots represent 0.50 s integrations, and the Moon took about 40 s to cross the aperture. (*c*) Differential photometry for the 1987 April 18 data. Same as (*a*), except that the software aperture is 1″.8, T_0 is 13^h47^m UT, the dots represent 0.260 s integrations, and the Moon took about 10 s to cross the software aperture.

Because the second half of the event was significantly affected by cloud, an attempt was made to remove this background from each frame. A two-dimensional second-order polynomial was fitted to each frame. The procedure allowed areas of the frame to be excluded from the fit, so appropriate boxes were placed round all the obvious genuine sources within the frames. A remarkable improvement in the cosmetic appearance of the frames resulted. The "gain" of each frame was then normalized to set the brightness of IRS 7 to be consistent with the value at the time it first emerged (when the Galactic center direction was free from cloud). All frames were then set to the same coordinate system by centroiding on IRS 7, so that effects of telescope guiding errors were reduced ~0.5 pixels.

Photometry on the various Galactic center sources was performed by placing "boxes" round them and measuring the

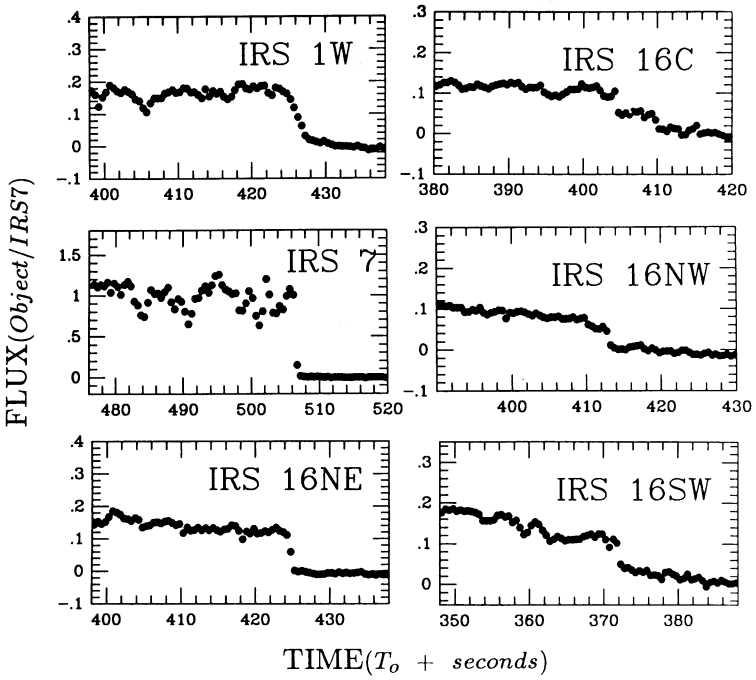

FIG. 2b

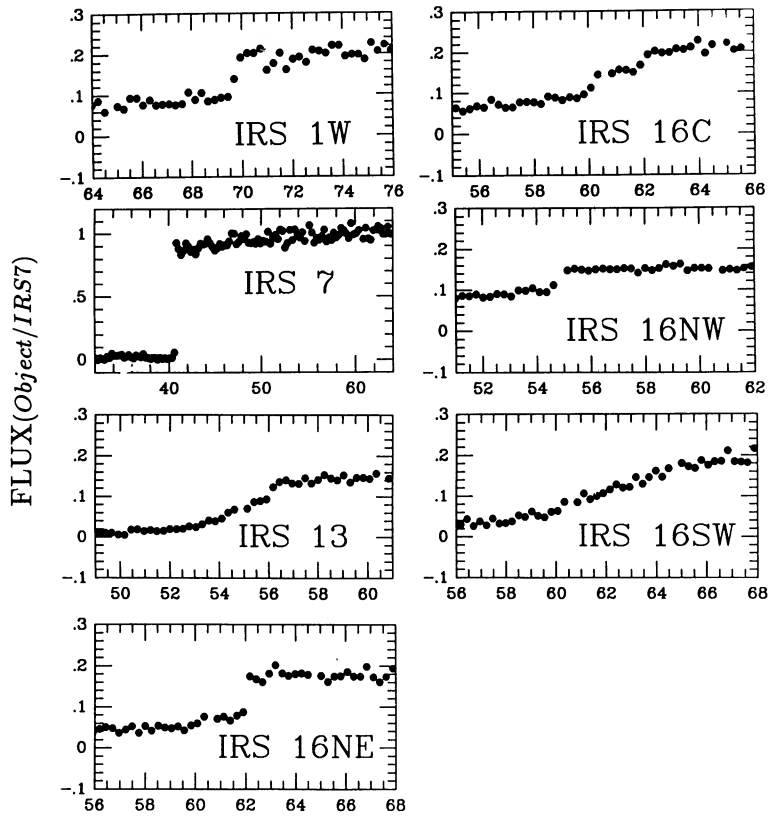

FIG. 2c

TABLE 3

1987 APRIL OCCULTATION CAMERA RESULTS

Object	Flux/IRS 7	m_K	Comments and Size
IRS 1W (total)	0.124 ± 0.013	9.0	Compact
IRS 7	1.0	6.8	Compact
IRS 13 (total)	0.135 ± 0.016	9.0	
IRS 16NE	0.109 ± 0.013	9.1	Compact
IRS 16C	0.080 ± 0.012	9.5	Compact
IRS 16SW (total)	0.200 ± 0.014	8.5	>0".6
IRS 16NW	0.063 ± 0.011	9.7	Compact

signal within each box. A first-order background subtraction was not necessary as the mean background had been set to zero during the polynomial fitting. A box size of 3 × 3 pixels (1".8 × 1".8) was chosen as the best compromise between resolving confused sources and sampling the seeing disk. Profiles of IRS 7 indicated that the seeing was ~2". Time series photometry was carried out by monitoring the flux from a box over the time taken for that region to be uncovered by the lunar limb. Additional frames were measured to determine the "before" and "after" levels of that region. Some examples of the IRCAM results are given in Figure 2*c*. There are a few gaps in the time series photometry shown in Figure 2*c*. The missing data points correspond to a few missing images. The results are summarized in Table 3, which is in the same format as Table 2. The photometric results are in good agreement with the results of the 1988 July and September observations and are compared explicitly in Table 4. FPS found $K = 10.0$ mag for IRS 16NW, in good agreement with other determinations. However, they found IRS 7 to $K = 6.4$ mag at the time of their observations. Some of the scatter in Table 4 could be attributable to variability of IRS 7.

d) The Camera Results

The method for flux measurement we have described is fundamentally different from other techniques for photometry in a crowded field (e.g., FPS; RRP; TCB) because an object is separated from the others by the occultation. The method is independent of the intensity distribution of the object, as long as it is smaller than the software aperture, and does not require a reference object assumed to be a point source. The fluxes measured by the occultation method are compared with previous determinations in Table 4. The object name is given in column (1); column (2) gives the magnitude difference with respect to IRS 7 determined from the 1987 April occultation, and column (3) gives corresponding quantity determined from the 1988 July and September data. The next four columns list measurements from BN, FPS, RRP, and TCB. The agreement is quite good between the two sets of camera observations. Their agreement with prior photometry is also quite good. The discrepancies are greatest for the components of IRS 16, which is not surprising because of the difficulty of photometry in a crowded field by the usual techniques.

The main results of the three camera observations are as follows:

a) IRS 1W: The 1988 July data (Fig. 2*a*) resolves IRS 1W into two components, IRS 1W-W and 1W-E with separation ~0".4 in the projection of this event. The component orientation must be roughly east-west, because they are not separated in either the 1988 September or 1987 April data (Figs. 2*b* and 2*c*), although in the former the two sources are oriented such that the flux takes four frames to disappear. The presence of two sources explains the TCB finding that IRS 1W was just barely resolved in their *K*-band image.

b) IRS 7: The signal-to-noise of the IRS 7 occultations is the best in the 1987 April and 1988 July events. A burst of bad seeing degraded the images just before the disappearance of IRS 7 in the 1988 September event (compare Figs. 2*a* and 2*c* with 2*b*). The analysis described in the Appendix indicates that, in the direction of the 1987 April and 1988 July events, IRS 7 is smaller than ~12 mas or ~100 AU.

c) IRS 7SE: With the software aperture centered 1".7 E and 0".9 S of IRS 7, the disappearance of IRS 7SE is seen in Figure 2*a* at ~$11^h17^m33^s.1$ UT. The flux decrease at ~$11^h17^m31^s.2$ is attributable to the disappearance of IRS 7.

d) IRS 13: The 1988 July data resolve IRS 13 into two objects: IRS 13E, which disappears at ~$11^h17^m22^s.6$, and 13W, which disappears at ~$11^h17^m20^s$. (The flux decrease resulting from the disappearance of 13E is also seen at the appropriate time in the panel labeled 13W [i.e., centered on IRS 13W] in Fig. 2*a*). In the projection of the July event, 13E and 13W are separated by ~1".2. The 1987 April data (Fig. 2*c*) suggests that IRS 13 consists of one pointlike and either an extended source or two other point sources. The extended source would be ~0".3 in extent. Comparing with the 1988 July data, the orientation of the definite point source to the extended/double source is such that the point source reappears last, thus to the south-east of the extended/double source.

e) IRS 16NE is compact. It is the strongest compact source of the IRS 16 cluster. The size upper bounds for nominal parameters of the events are 65 mas (1987 April), 60 mas (1988 July), and 25 mas (1988 September).

f) IRS 16 center (16C) is compact. Its occultations are seen

TABLE 4

COMPARISON OF FLUX DETERMINATIONS

	THIS WORK					
OBJECT (1)	1987 Apr (2)	1988 Jul/Sep (3)	BN (4)	FPS (5)	RRP (6)	TCB (7)
IRS 1W (total)	2.2	1.9	...	...	2.2	...
IRS 9	...	2.1	2.1	...	2.5	...
IRS 13 (total)	2.2	2.2	2.0	...	2.5	...
IRS 16NE	2.3	2.1	...	...	2.1	1.8
IRS 16SW (total)	1.7	2.0	...	...	2.1	1.4
IRS 16NW	2.9	3.3	...	3.6	2.2	3.4
IRS 16C	2.7	3.3	...	...	...	1.9

NOTE.—$\Delta m_K = m_K(\text{object}) - m_K(\text{IRS 7})$.

at $\sim 11^h17^m32^s.4$ UT in Figure 2*a*, $\sim 3^h16^m44^s$ in Figure 2*b*, and $\sim 13^h48^m0^s.5$ in Figure 2*c*.

g) IRS 16SW: The 1988 July data (Fig. 2*a*) show two components: a compact one, 16SW-W, which radiates about half the flux measured in the 2″ aperture, and an extended component, 16SWext. The flux of IRS 16SWext extends for ~1″ to the east of 16SW-W. To search for a discrete component that could be responsible for this emission, we carried out the time series photometry on the July data with the software aperture centered at several positions to the east of IRS 16SW-W. No discrete component could be identified to a level half that of IRS 16SW-W. The 1988 September data (Fig. 2*b*) also show 16SW-W clearly, but it is difficult to assess the extended structure because of the limb effects discussed in § III*b*. The 1987 April data (Fig. 2*c*) show clearly the emission of an extended component at least 0″.6 in extent.

h) IRS 16NW is compact.

i) All the other sources brighter than $K \sim 10$ mag are compact.

j) We searched for the emission of a compact component at the position of Sgr A*. No compact component could be identified to a flux limit 0.03 that of IRS 7, or $K \sim 10.6$ mag, at the 3 σ level.

IV. ANALYSIS OF HIGH-SPEED PHOTOMETRY

a) The Data

The data obtained during 20 s centered on the reappearance of IRS 16 are shown in Figure 3. In this figure, the original data points taken at 2 ms resolution are binned to 20 ms; segments of the data at the full 2 ms resolution are shown in Figure 5. The flux scale was calibrated by observing the occultations of stars of known flux. The absolute accuracy of the time scale is ± 1 s. The relatively large and fast increases of the signal are caused by the reappearances of discrete objects. The systematic slow flux increase shows that a significant fraction of the flux within the aperture arises in extended emission. Our goals are to use these data to obtain improved angular size determination for the discrete sources and to determine the flux and some information about the angular extent of the diffuse emission. The analysis is complicated, however, by the faintness of the discrete components, their distribution within the beam, and the extended structure.

The data were analyzed by a combination of deconvolution and modeling. Estimates of the intensity distribution and noise obtained by deconvolving the data at relatively coarse angular resolution are described in § IV*b*. After the discrete components were identified, their fluxes were measured directly from the high-speed photometry data (§ IV*c*), and size estimates were obtained by modeling segments of the data (§ IV*d*).

b) Identification of the Source Components

The occultation data were deconvolved using the Richardson-Lucy (R-L) algorithm (Richardson 1972; Lucy 1974). The R-L algorithm is well suited for the inversion of occultation data because it is insensitive to noise (Richichi, Salinari, and Lisi 1988; Chen 1990; Chen *et al.* 1990). Two inversion solutions were calculated. In the first, the 20 s of data containing the reappearance of IRS 16 were analyzed. To expedite the calculation, the data points were binned to 20 ms. The calculated intensity distribution is shown in Figure 3*b*. The intensity distribution is the projection of the two-dimensional intensity distribution within the beam along the occultation direction. Figure 4 shows the solution plotted adjacent to a map of the region at the correct scale and orientation and aligned to provide the best correspondence between the strongest peaks and the components of IRS 16. IRS 16 NE, C, and SW-W are easily identified. An exact correspondence cannot be expected because the lunar limb is not smooth. The calculated intensity distribution also shows extended low–surface brightness emission.

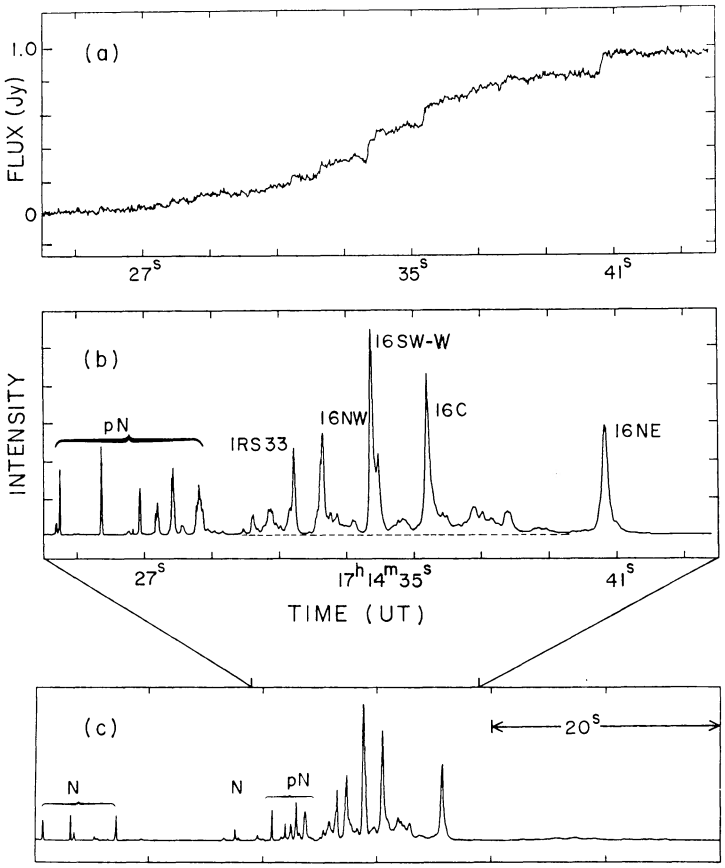

FIG. 3.—(*a*) The flux detected in a 6″ aperture centered on IRS 16 as the Moon uncovered the region (see also Fig. 4). The original data were a series of 2 ms integrations. Here the data were binned so each point represents 20 ms. It took about 18 s for the Moon to cross the aperture. (*b*) The one-dimensional intensity distribution calculated from the 20 ms binned data in (*a*) using the Richardson-Lucy algorithm. The peaks corresponding to the components of IRS 16 and IRS 33 are labeled. (*c*) An inversion solution of the full 1 minute of data binned to 60 ms per point. The features labeled "N" and "pN" are noise and probably noise, respectively.

Not all features of the solution are real. The origin of noise features can be identified easily. They are caused by a signal increase followed by a decrease that are slower than the rapid fluctuations characteristic of electronic noise. Examples are seen around $17^h14^m31^s$ and $17^h14^m38^s$ UT in Figure 3*a*. The decreases are obviously noise because the signal should generally increase, or hold steady, as IRS 16 reappears. We do not understand the origin of this type of noise. The likely possibilities include detector noise, atmospheric effects compounded by sunlight, image motion within the aperture, and effects of the lunar limb. Unfortunately, the flux increases can mimic the appearance of an object and because the R-L solutions are intrinsically positive, they will be recovered as features.

To estimate the effects of this noise, another solution for the

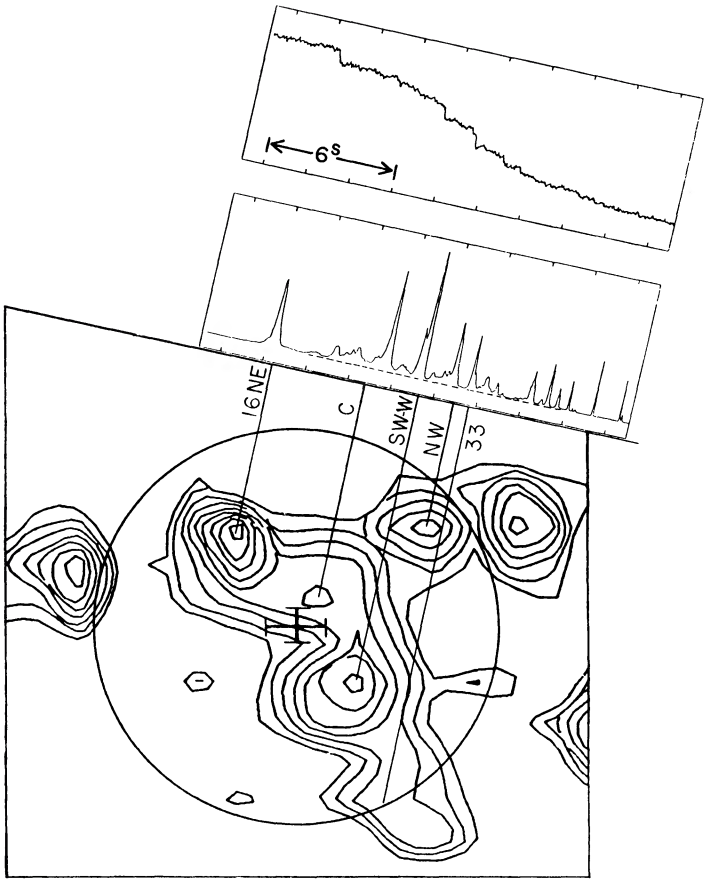

FIG. 4.—The set-up and results for the observation of the 1989 February 2 event by high-speed photometry. The image is the same as in Fig. 1, but is plotted to show only IRS 16. The circle represents the 6″ aperture centered ~6″ S and ~2″ E of IRS 7. Crossed error bars represent the uncertainty of the beam location, ±0″.5. The inversion solution shown in Fig. 3*c* is reproduced at the scale and orientation appropriate to this event.

full minute of data was calculated. Any features showing up in the first or last ~20 s of this solution must be spurious because they are derived from data obtained when the Moon either completely covered the aperture or was completely out of it. For this calculation, the data points were binned to 60 ms. The result is shown in Figure 3*c*. The central 20 s of this solution reproduce most of the features of Figure 3*b*. However, the peaks marked "N" in the first 20 s of data must be noise. We therefore identify by "pN," for "probably noise," features of comparable area in the central 20 s and use this designation also in Figure 3*b*. The signal increase and decrease near $17^h41^m34^s$ UT, which has the effect making IRS 16 SW appear to have two components in the deconvolution, are probably both noise. The reappearances of IRS 16 NW and 33 are detected above these noise levels.

c) Fluxes and the Extended Emission

The most reliable way to measure the fluxes of the compact components seen in the high-speed photometry is to use the signal jumps caused by their reappearances. The fluxes determined from the high-speed photometry and the camera time series photometry are compared in Table 5. Column (2) lists the fluxes from the high-speed photometry. The camera photometry fluxes in column (3) are the average of the IRCAM and Rochester Camera results. The agreement is good.

TABLE 5

HIGH-SPEED PHOTOMETRY FLUXES

Object (1)	High-Speed Photometry (Jy) (2)	Camera Photometry (Jy) (3)
IRS 16NE	0.13 ± 0.02	0.15 ± 0.01
IRS 16SW-W	0.07 ± 0.02	0.10 ± 0.01
IRS 16C	0.09 ± 0.02	0.08 ± 0.01
IRS 16NW	0.06 ± 0.02	0.07 ± 0.01
IRS 33	0.06 ± 0.02	0.05 ± 0.01

The total flux detected in the 6″ aperture when the Moon fully uncovered the region is ~0.96 Jy. Subtracting from this the sum of the fluxes of the discrete components, we obtain that (0.48 ± 0.03) Jy, or about 50% of the total flux, arises in the extended component. The one-dimensional intensity distribution shows (Figs. 3*b* and 3*c*) that the extended component is not distributed uniformly within the aperture. In the projection of the 1989 February occultation, it extends for at least 3″, is associated with the IRS 16 cluster, and does *not* peak along the line of sight toward Sgr A*.

d) Sizes of the Compact Components

Sections of the data for IRS 16C, NE, and SW-W are shown in Figure 5. Our approach was to ignore the generally increasing signal of the distributed emission and to estimate the size of the compact components by model fitting the signal just at

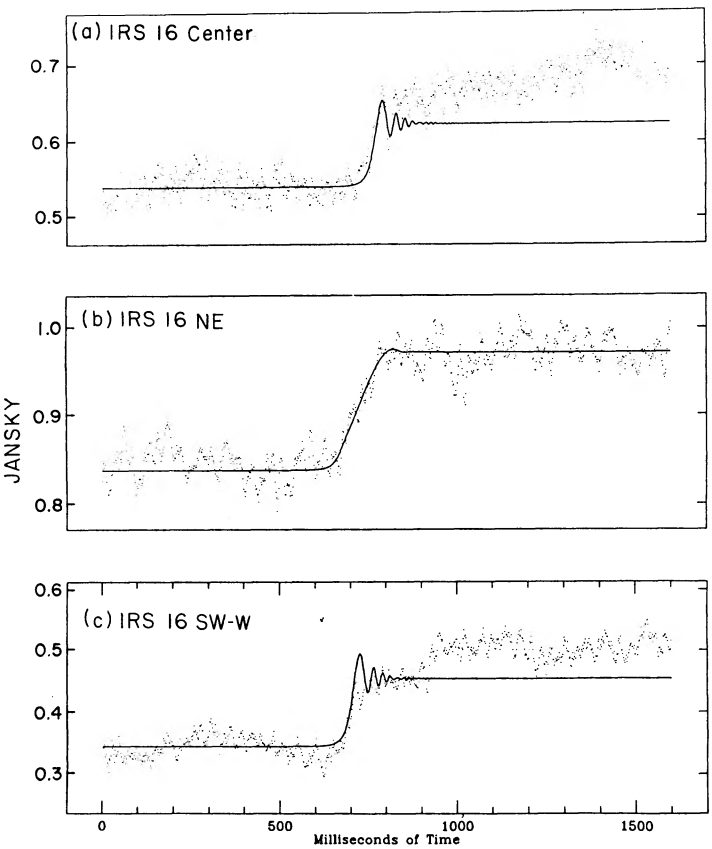

FIG. 5.—Segments of the original (2 ms) data at the times of the reappearances of (*a*) IRS 16C, (*b*) NE, and (*c*) SW, and (*solid lines*) the best fits obtained by modeling.

their reappearance using the identifications provided by the R-L calculation. The main criterion by which size was estimated was by the fit to the rise of signal during the reappearance.

IRS 16C.—The slowly increasing signal is prominent during the reappearance of IRS 16C. A Fresnel pattern is seen which is best modeled by a pointlike object at the nominal rate. Since the fit produced by a 10 mas object is noticeably worse, we set 10 mas as the upper bound for the size of IRS 16C.

IRS 16NE.—The duration of the reappearance (Fig. 5*b*) is ~170 ms which, using the nominal rate and geometric optics, implies an angular size of ~55 mas. An alternative explanation of the data would be a more compact source occulted at a slower rate. We think this is unlikely, because no Fresnel fringes are seen for a compact object. The extreme case of a pointlike object would require a rate of 0.05 arcsec s^{-1}. This would imply a limb slope of ~60°, which is improbably large. The ~55 mas size implied by the high-speed photometry is a problem because it is in conflict with all our camera data, which set upper bounds of comparable size. The situation is discussed further in § V*a*, where all our data for IRS 16NE are considered together.

IRS 16SW-W.—The signal increase is best fitted as the reappearance of an unresolved object at the nominal rate. As for IRS 16C, we set an upper bound of 10 mas on the size. An example of the spurious flux increase and decrease discussed in § IV*b* is seen just after the reappearance.

V. DISCUSSION

*a) The Discrete Sources near Sgr A**

IRS 16SW-W and C are smaller than 10 mas (85 AU). IRS 16NW and IRS 29 are smaller than 60 mas (510 AU). The camera and high-speed photometry results for IRS 16NE are summarized in Figure 6. The three camera observations do not resolve it, while the the high-speed photometry appears to set a size of 55 mas. The nominal occultation directions of the 1988 July event, which sets an upper bound of 60 mas, and the event observed by high-speed photometry (1989 February), are very nearly the same. Thus, it would take a very peculiar geometry to reconcile the four observations if they were taken at face value. The sources of noise described in § IV*b* could make a unresolved object appear resolved. We believe, therefore, that the most consistent and conservative interpretation of our four observations is that IRS 16NE is unresolved and smaller than 60 mas (510 AU) in the directions of the four observations.

Adams *et al.* (1988) identified IRS 16NE with a resolved feature ~0".3 in extent. Inspection of their Figure 1 shows that, for the geometry of the La Palma event, the lunar limb crossed IRS 16NE and the extended emission to the east of 16SW-W nearly simultaneously. In view of the results described here, it seems likely that most of the extent that Adams *et al.* assigned to 16NE is in fact attributable to 16SWext. Earlier in the La Palma event, IRS 16 C and 16SW-W were superposed and thus similarly difficult to unravel.

Thus, one of the main results of this work is that all the discrete objects near Sgr A* are very small. It is difficult to imagine how clusters of stars could be contained within dimensions as small as 85–500 AU. It seems most likely that these objects are stars or systems of a few stars. Estimates of the *K*-band extinctions to stars in the central parsec of the Galaxy are in the range $A_K = 2.7$ (Becklin *et al.* 1978) to $A_K = 3.5$ mag (RRP for $A_V = 31$). At an assumed distance of 8.5 kpc, the M_K values of the components of IRS 16 are thus −7 to −9 mag. Moreover, RRP estimated that the components of IRS 16 may be very blue. A relatively few very luminous stars thus could be responsible for the luminosity and ionizing flux at the center of the Galaxy. They could well be Wolf-Rayet stars (Forrest *et al.* 1987; Werner and Stauffer 1988; Allen *et al.* 1989).

All our camera data show a region of diffuse *K*-band emission IRS 16SWext extending for 0".5–1" to the east of IRS 16SW-W. At 3.5 μm, TCB resolved 16SW into two components, SW-W and SW-E, separated by 0".8 east-west with SW-W the brighter. The TCB 2.2 μm map also resolves only SW-W. The relationship of the extended source SWext seen at 2.2 μm to SW-E delineated at 3.5 μm by TCB is unclear.

b) Other Stars in the Central Parsec of the Galaxy

IRS 1W, 10, and 13 are associated with enhancements of free-free emission detected in radio images (Morris and Yusef-Zadeh 1987; Yusef-Zadeh 1988) and hydrogen Brα line emission (Forrest *et al.* 1987). Our observations show IRS 1W and IRS 13 are each resolved into two objects. They are probably the stars exciting these H II regions.

The differential luminosity function of the stars in the central 5′ × 5′ of the galaxy (the central ~150 pc^2), in terms of the apparent *K* magnitude is shown in Figure 7*a* (Lebofsky and Rieke 1987; Rieke 1989). It peaks around $m_K \sim 10.5$ mag. The luminosity function derived from the present results for the central parsec is also shown in Figure 7*b*. The luminosity functions for the two areas may be compared directly because the *K*-band extinction is very roughly the same over the central 5′ × 5′ region (Lebofsky and Rieke 1987). The luminosity function of the central parsec shows a sharp drop at $m_K > 10.5$ mag. The difficulty of identifying faint sources in a crowded

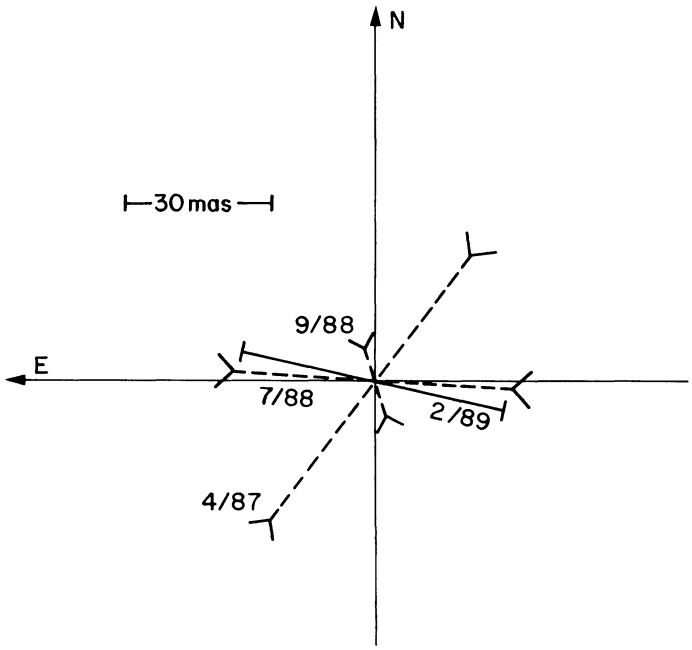

FIG. 6.—A summary of our results for IRS 16NE. The length of the dashed lines represent the angular size upper bounds derived from the camera observations. Their direction represents the nominal occultation directions. The solid line represents the measurement derived from the high-speed photometry. We consider IRS 16NE unresolved and set 60 mas as an upper limit on its size (§ V*a*).

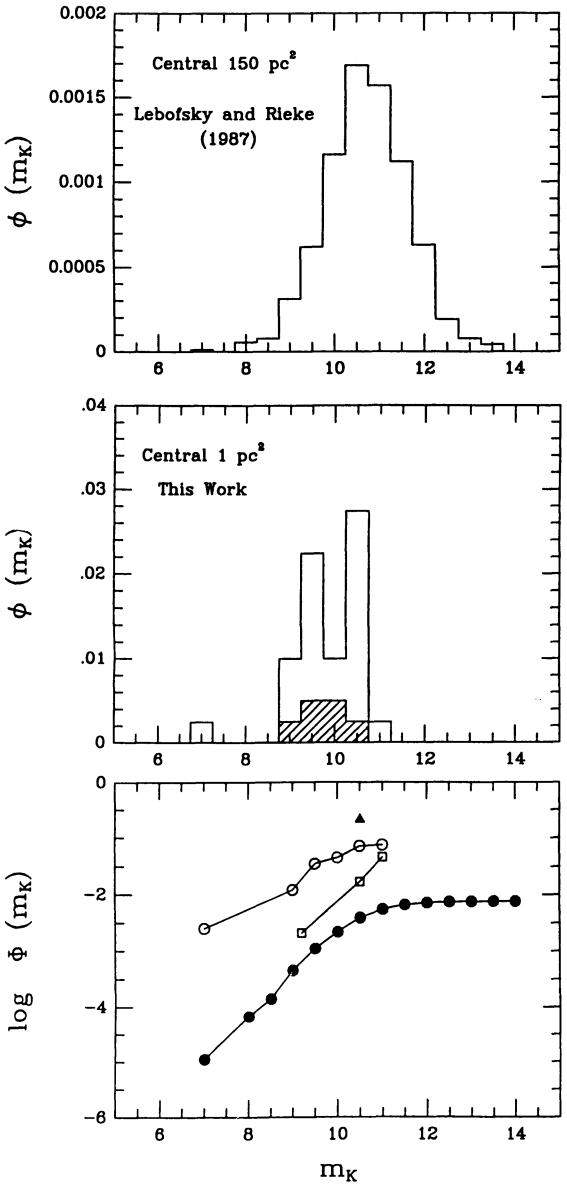

FIG. 7.—(*top*) The histogram is the differential luminosity function in terms of apparent K magnitude for the stars in the central 150 pc^2 of the galaxy (Lebofsky and Rieke 1987; Rieke 1989). The units are stars per square arcsec per half-magnitude interval. (*middle*) The differential luminosity function for the central pc^2 determined from the data in Table 2 (but omitting IRS 16SWext). The units are the same as in the top panel, and the luminosity function refers to an area of 402 arcsec^2 (referring to Fig. 1, the strips within $\sim$1.″5 of the northern, eastern, and southern borders and the region obscured by the Moon were not included). The hatched aras represent IRS 16NE, C, SW-W, NW, and IRS 29 and 33, the objects within 3″ radius of Sgr A*. (*bottom*) The integral luminosity function (in units of number per square arcsec) for the central 5′ as derived from the data of Lebofsky and Rieke in the tope panel (*filled circles*), for an annulus centered on IRS 16 with inner radius 10″ and outer radius 20″ (Allen, Hyland, and Jones 1983) (*open squares*), the central $\sim$20″ derived from the middle panel (*open circles*), and for the objects within 3″ radius of Sgr A* (*solid triangle*).

field must account for some of the observed decrease. (Rieke 1989 notes that some of the decrease in the luminosity function at the faint end for the central 5′ × 5′ may be attributable to the requirement that the stars included in their study be detected at both H and K). The shapes of the luminosity functions for the central pc and the larger area appear similar at $m_K < 10.5$ mag. This suggests that the turnover in the luminosity function of the central pc at $m_K > 10.5$ is attributable not only to source confusion but also to the luminosity function itself.

The cross-hatching in Figure 7*b* represents IRS 16NE, C, SW-W, NW, IRS 29, and IRS 33, the objects within 3″ radius of Sgr A*. Their distribution of apparent K-band flux is not significantly different from that of the stars in the central parsec of the Galaxy. The real density of the stars in the central 6″ is, however, about 3 times greater than the average for the central parsec (Fig. 7*c*). Furthermore, the areal star density in the central parsec is about twice that in an annulus of radii between 10″ and 20″ centered on IRS 16 that was analyzed by Allen, Hyland, and Jones (1983). Thus, a steady increase of star density toward the center of the Galaxy is observed.

c) Diffuse Emission

The high-speed photometry shows that $\sim$0.48 Jy in a 6″ beam centered on IRS 16 arises in unresolved emission. Adams *et al.* (1988) obtained a similar result. Figure 4 shows that most of this emission arises within the central 3″ and that it is not centered on Sgr A*. Free-free and bound-free emission of the ionized gas in this region cannot account for the measured flux. Scaling from the radio emission included in the 6″ aperture (Morris and Yusef-Zadeh 1987; Yusef-Zadeh 1988) according to H II region theory for a temperature of 10^4, a flux density of 0.2–0.4 Jy at K is obtained. Extinction of about 3 mag at 2 μm (§ V*a*) would reduce this to 12–25 mJy.

To investigate whether the unresolved emission could come from faint stars in a cluster near the center of the Galaxy, we assumed that the luminosity function of such stars at $m_K >$ 10.5 followed the shape of the distribution determined by Lebofsky and Rieke (1987). About 16 stars with m_K between 10.5 and 14 mag could produce the observed unresolved K-band emission. This would require an areal star density about 12 times higher than the average for the central parsec, but only 4 times higher than the average for the central 6″. This concentration of stars seems plausible and provides a natural explanation for the unresolved emission.

VI. SUMMARY

We have observed four separate lunar occultations of the Galactic center in the infrared K-band. Three of the observations were by infrared cameras. The fourth was by high-speed photometry through an aperture centered on the IRS 16 cluster. We used these observations to estimate the size of the sources and to derive photometry. We find that:

1. IRS 16NE, 16NW, and IRS 29 are smaller than $\sim$510 AU and IRS 16SW-W and C are smaller than 85 AU.
2. To the east of 16SW-W there is a faint emission region, 16SWext. It appears 0.″5–1″ in extent. The nature of this component is not clear.
3. All sources brighter than $K = 10$ mag in the central pc are smaller than 510 AU and therefore seem to be stars.
4. IRS 7 is smaller than $\sim$100 AU.
5. IRS 1W and 13 were resolved into pairs of stars. They are probably the exciting stars for these H II regions.
6. About half the total flux detected from the IRS 16 region is unresolved. The diffuse emission is not centered on Sgr A*. It probably arises in an unresolved cluster of faint stars.
7. The shape of the differential luminosity function of the

stars in the central pc^2 is similar to that for the stars in the central 150 pc^2 (Lebofsky and Rieke 1987).

8. There is a steady increase of star density toward the central few arcseconds of the galaxy.

Observing occultations of the Galactic center has been fun. We thank the Saros, however, for arranging that they occur only every 18 years. Eric Becklin, Bob Howell, Doug Simons, and Doug Toomey helped many, many times throughout this campaign; it is a pleasure to thank them. Detailed comments by the referee, Eric Becklin, and Doug Simons helped us improve this paper. We thank Bob McLaren for permitting the CFHT to operate under marginal conditions. We thank D. J. Adams, R. F. Jameson, I. S. McLean, C. Aspin, and I. Smith for their particular efforts in getting the fast photometry mode of IRCAM operational. We thank Judy Pipher and Zoran Ninkov for help with the Rochester IR camera, Marcia Rieke for providing the luminosity function of the central 5′ × 5′ in terms of apparent magnitude, Farhad Yusef-Zadeh for sending to us high-resolution radio maps in advance of publication, and Leonid Ozernoy for helpful discussions. We thank the directors and time allocation committees of the CFHT, IRTF, and UKIRT for assigning time to this project and the observatory staffs for their thorough support. M. S. acknowledges the support of a Fullam Award and the NSF. W. F. acknowledges the support of the NSF, the National Geographic Society, and NASA–Ames. R. I. D. is in receipt of an SERC postgraduate studentship.

APPENDIX

SIZE ESTIMATE FOR CAMERA OBSERVATION OF THE OCCULTATION OF A BRIGHT OBJECT

Consider the disappearance of a bright point source object in the limit of geometric optics so Fresnel diffraction can be ignored. There will, in general, be at least one image in which the signal is intermediate between the full value seen before the disappearance, and the zero signal afterwards. Let $\Delta\theta_m$ equal the angular distance advanced by the limb in an integration. The signal is proportional to the flux and the length of time the object is visible and thus depends on where the object lies within $\Delta\theta_m$. The intermediate value of the signal will be nearly the full value if the object is positioned "late" within $\Delta\theta_m$, and nearly zero if it is positioned "early." The average of the intermediate value of the observation of many point objects should be half the full value. Next consider an object whose size is exactly $\Delta\theta_m$. If its position on the sky is such that it starts to be obscured exactly as an integration starts, then there will be one intermediate signal value at half the full value. If the object is not so fortuitously positioned, then there will be two images with intermediate values of the signal. If the object is bigger than $\Delta\theta_m$, there will be more than two images having intermediate signal values.

If an object disappears so there is only one image with an intermediate signal that is f of the full value, then an upper limit $\Delta\phi$ can be set on its size:

$$\Delta\phi \leq (f/0.5)\Delta\theta_m \quad \text{if } f < 0.5 ,$$

or

$$\Delta\phi \leq (1-f)/0.5\,\Delta\theta_m \quad \text{if } f > 0.5 .$$

Figure 2*a* shows that IRS 7 in the 1988 July data disappeared with one intermediate value image at $f \sim 0.1$. Using the nominal occultation rate for this event, $\Delta\theta_m \sim 60$ mas so the size of IRS 7 in the east-west direction is ≤ 12 mas, or ≤ 100 AU.

REFERENCES

Adams, D. J., Becklin, E. E., Jameson, R. F., Longmore, A. J., Sandqvist, Aa., and Valentijn, E. 1988, *Ap. J. (Letters)*, **327**, L65.
Allen, D. A., Hyland, A. R., Hillier, D. J., and Bailey, J. A. 1989, in *The Center of the Galaxy*, ed. M. Morris (Dordrecht: Kluwer), p. 513.
Allen, D. A., Hyland, A. T., and Jones, T. J. 1983, *M.N.R.A.S.*, **204**, 1145.
Backer, D. C., and Sramek, R. 1987, in *The Center of the Galaxy*, ed. M. Morris (Dordrecht: Kluwer), p. 163.
Becklin, E. E., Matthews, K., Neugebauer, G., and Willner, S. P. 1978, *Ap. J.*, **220**, 831.
Becklin, E. E., and Neugebauer, G. 1975, *Ap. J. (Letters)*, **200**, L71 (BN).
Chen, W. P. 1990, in preparation.
Chen, W. P., Simon, M., Longmore, A. J., Howell, R. R., and Benson, J. A. 1990, *Ap. J.*, **357**, 224.
Evans, D. S., and Edwards, D. A. 1980, *A.J.*, **86**, 1277.
Forrest, W. J., Pipher, J. L., and Stein, W. A. 1986, *Ap. J. (Letters)*, **301**, L49 (FPS).
Forrest, W. J., Shure, M. A., Pipher, J. L., and Woodward, C. E. 1987, in *The Galactic Center*, ed. D. C. Backer (*AIP Conf. Proc. No. 155*), p. 153.
Kerr, F. J., and Lynden-Bell, D. 1986, *M.N.R.A.S.*, **221**, 1023.
Lebofsky, M. J., and Rieke, G. H. 1987, in *The Galactic Center*, ed. D. C. Backer (*AIP Conf. Proc. No. 155*), p. 79.
Lucy, L. B. 1974, *A.J.*, **79**, 745.
McGinn, M. T., Sellgren, K., Becklin, E. E., and Hall, D. N. B. 1989, *Ap. J.*, **338**, 824.
McLean, I. S., Aspin, C., Longmore, A. J., and Dixon, R. I. 1987, in *Infrared Astronomy with Arrays*, ed. C. G. Wynn-Williams, E. E. Becklin, and L. H. Good (Honolulu: University of Hawaii), p. 321.
Morris, M., and Yusef-Zadeh, F. 1987, in *The Galactic Center*, ed. D. C. Backer (*AIP Conf. Proc. No. 155*), p. 127.
Richardson, W. H. 1972, *J. Opt. Soc. Am.*, **62**, 55.
Richichi, A., Salinari, P., and Lisi, F. 1988, *Ap. J.*, **326**, 791.
Rieke, G. H., Rieke, M. J., and Paul, A. E. 1989, *Ap. J.*, **336**, 752 (RRP).
Rieke, M. 1989, private communication.
Simons, D. A., Becklin, E. E., and Hodapp, K.-W. 1989, in *The Center of the Galaxy*, ed. M. Morris (Dordrecht: Kluwer), p. 509.
Simons, D. A., Hodapp, K.-W., and Becklin, E. E. 1990, *Ap. J.*, **360**, 106.
Tollestrup, E. V., Capps, R. W., and Becklin, E. E. 1989, *A.J.*, **98**, 204 (TCB).
Werner, M. W., and Stauffer, J. R. 1988, *Bull. AAS*, **20**, 1097.
Yusef-Zadeh, F. 1988, private communication.

W. P. Chen and M. Simon: Astronomy Program, State University of New York, Stony Brook, NY 11794

R. I. Dixon: Department of Astronomy, Edinburgh University, Blackford Hill, Edinburgh EH9 3HJ, Scotland, UK

W. J. Forrest and J. D. Garnett: Physics and Astronomy Department, University of Rochester, Rochester, NY 14627

T. Gauer and A. J. Longmore: Royal Observatory, Blackford Hill, Edinburgh EH9 3HJ, Scotland, UK